$(g-2)$ anomalies and neutrino mass

Carolina Arbeláez,[1,*] Ricardo Cepedello,[2,†] Renato M. Fonseca,[3,‡] and Martin Hirsch[2,§]

[1]*Universidad Técnica Federico Santa María and Centro Científico Tecnológico de Valparaíso CCTVal, Casilla 110-V, Valparaíso, Chile*

[2]*Instituto de Física Corpuscular (CSIC-Universitat de València), C/ Catedrático José Beltrán 2, E-46980 Paterna (València), Spain*

[3]*Institute of Particle and Nuclear Physics, Faculty of Mathematics and Physics, Charles University, V Holešovičkách 2, 18000 Prague 8, Czech Republic*

(Received 30 July 2020; accepted 17 September 2020; published 8 October 2020)

Motivated by the experimentally observed deviations from standard model predictions, we calculate the anomalous magnetic moments $a_\alpha = (g-2)_\alpha$ for $\alpha = e, \mu$ in a neutrino mass model originally proposed by Babu, Nandi, and Tavartkiladze (BNT). We discuss two variants of the model: the original model, and a minimally extended version with an additional hypercharge-zero triplet scalar. While the original BNT model can explain a_μ, only the variant with the triplet scalar can explain both experimental anomalies. The heavy fermions of the model can be produced at the high-luminosity LHC, and in the part of parameter space where the model explains the experimental anomalies it predicts certain specific decay patterns for the exotic fermions.

DOI: 10.1103/PhysRevD.102.075005

I. INTRODUCTION

Apart from neutrino masses, as observed in oscillation experiments [1,2],[1] there are only a few experimental hints for new physics. Among them is the long-standing deviation of the anomalous magnetic moment of the muon from the standard model (SM) prediction [5].

Currently, the experimental data gives a roughly 4σ C.L. deviation [6–12] from the SM prediction[2]:

$$\Delta a_\mu = (27.06 \pm 7.26) \times 10^{-10}. \tag{1}$$

Two new experiments will shed light on this tension: the E989 experiment at Fermilab [14] and E34 at J-PARC [15]. E989 (running since 2018) and E34 (planned to start in 2024) will improve the experimental accuracy by a factor of 4 and 5, respectively, leading to a 5σ C.L., in case the central value of the older measurement is confirmed.

From the theory side, there is still a debate about the SM calculation of the anomalous magnetic moment regarding hadronic vacuum polarization (HVP). A recent lattice-QCD result [16] for HVP brought the SM prediction of $(g-2)$ of the muon into agreement with experiments. However, this result is in tension with $e^+e^- \to$ hadrons cross-section data and global fits to electroweak precision observables [17].

More recently, a new precise measurement of the fine-structure constant [18] led to a deviation in the $(g-2)$ of the electron [19],

$$\Delta a_e = -(8.7 \pm 3.6) \times 10^{-13}. \tag{2}$$

Although less significant (roughly 3σ C.L.), it provides a new motivation to study $(g-2)$, as one might hope that both discrepancies have a common new physics origin. While both anomalies can be *easily* explained individually, the relative sign between a_μ and a_e makes it more complicated to find a common explanation. Simple Z' (dark photon) models cannot account for both discrepancies [20]. Several papers studying both anomalies in different contexts can be found in the literature [21–38].

In this paper we study $(g-2)$ and the electric dipole moment (EDM) for the electron and muon in the context of the Babu-Nandi-Tavartkiladze (BNT) model [39] and a simple extension of it. The BNT neutrino mass

*carolina.arbelaez@usm.cl
†ricepe@ific.uv.es
‡fonseca@ipnp.mff.cuni.cz
§mahirsch@ific.uv.es

[1]For a recent global fit to neutrino oscillation data see, for example, Refs. [3,4].

[2]After submitting our draft to the arXiv, it was brought to our attention that deviations between experiment and theory in $(g-2)_\mu$ have a surprisingly long history [13].

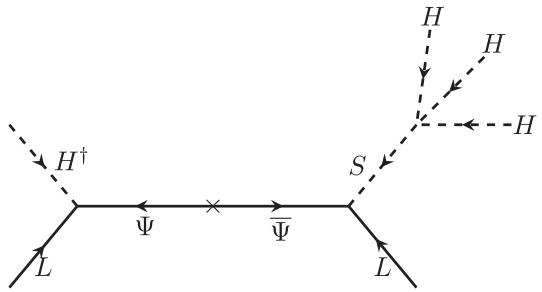

FIG. 1. Dimension-seven diagram responsible for neutrino masses in the BNT model.

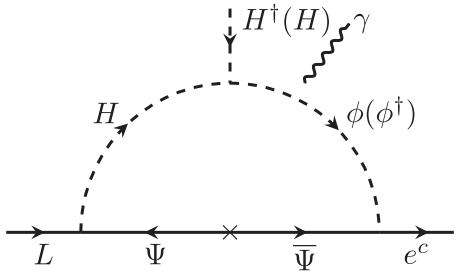

FIG. 3. Main contribution to the electromagnetic dipole moment operator in the BNTϕ model. Note that the photon line can be attached to any of the internal scalars or the fermion line.

model adds to the SM particle content vector-like fermion pairs $(\Psi, \bar{\Psi})$, which transform as $SU(2)_L$ triplets, and a scalar quadruplet S. With these fields neutrino masses are induced at tree level by a dimension-seven operator via the diagram shown in Fig. 1. By closing a pair of external scalar lines, a dimension-five operator can also be generated with a loop.

However, with this particle content the Wilson coefficient $c_R^{\alpha\beta}$ of the electromagnetic (effective) dipole moment operator, i.e.,

$$c_R^{\alpha\beta}\bar{\ell}_\alpha\sigma_{\mu\nu}P_R\ell_\beta F^{\mu\nu} + \text{H.c.}, \tag{3}$$

is suppressed by the small charged SM lepton masses, as can be seen from the diagrams in Fig. 2. Therefore, this model struggles to explain the current experimentally measured value of $(g-2)_\mu$, which significantly differs from the SM value. To do so very large values for Yukawa couplings are required, which are close to the edge of nonperturbativity, given current limits on the exotic fermion masses; see Sec. IV.

As can be seen in Eq. (3), a chirality flip (mass insertion) is needed to close the effective operator. While the particle content of the original BNT model requires a Higgs insertion on the SM lepton line, the situation changes with the addition of an extra (complex) scalar triplet ϕ with no hypercharge. A summary of the extra fields in this extended BNT model—henceforth referred to as BNTϕ—can be found in Table I. With this field content, the main contribution to the electromagnetic dipole moment operator becomes proportional to the mass of the heavy fermions $(\Psi, \bar{\Psi})$ rather than the muon mass, as shown in Fig. 3 (diagram in the electroweak basis).

The rest of the paper is organized as follows. In Sec. II we describe in detail the BNTϕ model. We derive the neutrino masses and the relevant mixings for the calculation of the Wilson coefficient $c_R^{\alpha\beta}$, directly related to $(g-2)$, the EDM, and $\text{Br}(\ell_\beta \to \ell_\alpha\gamma)$. At the end of the section we derive an analytical approximation for $c_R^{\alpha\beta}$, to provide some insight into the parameter dependence of the different observables. In Sec. III we give and analyze the main results for the BNT and BNTϕ models to compare both. We show that while the BNTϕ model can explain both anomalous magnetic moments fulfilling the experimental constraints, the BNT model can only account for $(g-2)_\mu$ with values for the Yukawas at the edge of perturbativity. In Sec. IV we study the phenomenology of both models at colliders for the parameter space where they explain neutrino masses and the anomalous magnetic moments. We finally close with a short discussion of our results. Only the most relevant pieces of the Lagrangian are given in the main text. The full Lagrangian can be found in the Appendix.

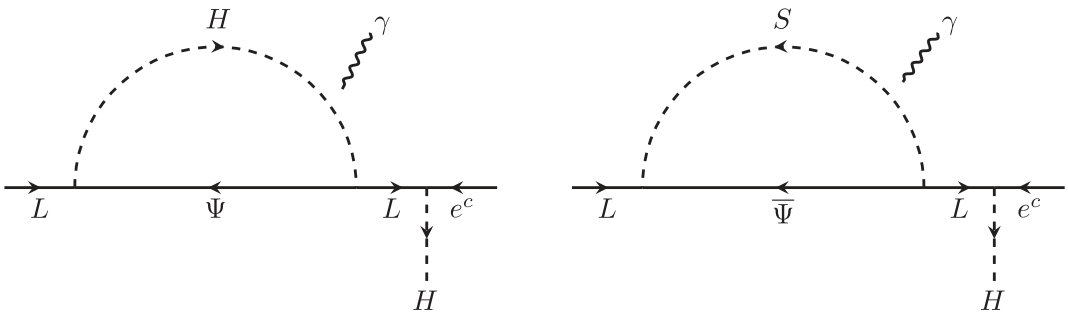

FIG. 2. Diagrams responsible for the electromagnetic dipole moment operator in the BNT model. Note that the photon line can be attached to the internal scalar or fermion line.

TABLE I. Quantum numbers of the new fields in the extended BNT model, namely, BNTϕ. It contains the complex ϕ scalar which is not part of the original BNT model. The Weyl fermions Ψ and $\bar{\Psi}$ are unrelated (the bar in $\bar{\Psi}$ is simply a reminder that it has the opposite quantum numbers of Ψ). One can have any number of generations of vector fermions $(\Psi, \bar{\Psi})$; for simplicity, we fix the number of copies to three.

	Spin	$SU(3)_c$	$SU(2)_L$	$U(1)_Y$
Ψ	$\frac{1}{2}$	**1**	**3**	1
$\bar{\Psi}$	$\frac{1}{2}$	**1**	**3**	-1
S	0	**1**	**4**	$\frac{3}{2}$
ϕ	0	**1**	**3**	0

II. MODEL SETUP

A. Lagrangian, masses, and mixings

We start by establishing a notation for the $SU(2)_L$ components of each field. We will assume that the components of L and H are organized in vectors,

$$L = \begin{pmatrix} \nu \\ \ell^- \end{pmatrix} \quad \text{and} \quad H = \begin{pmatrix} H^+ \\ H^0 \end{pmatrix}, \tag{4}$$

while the triplets Ψ, $\bar{\Psi}$, and ϕ are matrices:

$$\Psi = \begin{pmatrix} \frac{\Psi^+}{\sqrt{2}} & \Psi^{++} \\ \Psi^0 & -\frac{\Psi^+}{\sqrt{2}} \end{pmatrix}, \qquad \bar{\Psi} = \begin{pmatrix} \frac{\bar{\Psi}^-}{\sqrt{2}} & \bar{\Psi}^0 \\ \bar{\Psi}^{--} & -\frac{\bar{\Psi}^-}{\sqrt{2}} \end{pmatrix},$$
$$\text{and} \quad \phi = \begin{pmatrix} \frac{\phi^0}{\sqrt{2}} & \phi^+ \\ \phi^- & -\frac{\phi^0}{\sqrt{2}} \end{pmatrix}. \tag{5}$$

Last, S is taken to be a three-index symmetric tensor with the following components: $S_{111} = S^{+++}$, $S_{112} = S_{121} = S_{211} = S^{++}/\sqrt{3}$, $S_{122} = S_{212} = S_{221} = S^+/\sqrt{3}$, and $S_{222} = S^0$. The neutral scalars have nonzero vacuum expectation values (VEVs), which we will denote as $\langle H^0 \rangle \equiv v_H/\sqrt{2}$, $\langle \phi^0 \rangle \equiv v_\phi/\sqrt{2}$, and $\langle S^0 \rangle \equiv v_S/\sqrt{2}$. The electroweak bosons acquire masses $m_W^2 = g^2(v_H^2 + 4v_\phi^2 + 3v_S^2)/4$ and $m_Z^2 = (g^2 + g'^2)(v_H^2 + 9v_S^2)/4$, and therefore at tree level the ρ parameter has the value $(v_H^2 + 4v_\phi^2 + 3v_S^2)/(v_H^2 + 9v_S^2)$. In order for this number to not be far from unity, it follows that v_S and v_ϕ need to be much smaller than v_H. Indeed, assuming that only one of these two VEVs is different from zero and using data from Ref. [8], the 3σ upper limits for $|v_\phi|$ and $|v_S|$ are roughly 4 and 2 GeV, respectively.

On top of the SM couplings, the BNTϕ model contains the following mass and interaction terms:

$$\mathcal{L}_{\text{BNT}\phi} = M_\Psi \Psi\bar{\Psi} + Y_\Psi L\Psi H^* + Y_{\bar{\Psi}}\bar{\Psi}LS + Y_{e\phi} e^c \bar{\Psi}\phi + Y_{e\phi^c} e^c \bar{\Psi}\phi^* + Y_{\Psi\phi}\Psi\bar{\Psi}\phi + Y_{\Psi\phi^c}\Psi\bar{\Psi}\phi^* - \mathcal{V}, \tag{6}$$

$$\mathcal{V} = m_S^2 S^* S + m_\phi^2 \phi^*\phi + (\mu_\phi^2 \phi\phi + \mu_{H\phi} H^* H\phi + \lambda_5 S^* HHH + \lambda_9 H^* H\phi\phi + \text{H.c.}) + \lambda_{6a}(H^* H\phi^*\phi) + \lambda_{6b}(H^* H\phi^*\phi)' + \cdots. \tag{7}$$

We have omitted $SU(2)_L$ indices, as well as several scalar interactions which are of little importance for this work. Nevertheless, the full Lagrangian is displayed in the Appendix. Flavor indices can be read from the equations above with the understanding that the coupling matrices have indices ordered according to the position of the fermions; for example, $Y_\Psi L\Psi H^* = (Y_\Psi)_{ij} L_i \Psi_j H^*$. Note that, even though several parameters in the potential could be complex, in our numerical studies we will take them to be real for simplicity and allow complex entries only in the Yukawa matrices.

From the requirement that the first derivative of the potential is null for the nonzero vacuum expectation values v_H, v_ϕ, and v_S, together with the expected hierarchy of these VEVs, we get the approximate tadpole equations:

$$\mu^2 \approx -\frac{\lambda_1 v_H^2}{2} + 2(m_\phi^2 + 2\mu_\phi^2)\frac{v_\phi^2}{v_H^2}, \tag{8}$$

$$\lambda_5 \approx -2\frac{m_S^2}{v_H^3} v_S, \tag{9}$$

$$\mu_{H\phi} \approx 2v_\phi \frac{m_\phi^2 + 2\mu_\phi^2}{v_H^2}. \tag{10}$$

In the very first equation, μ^2 and λ_1 are the SM scalar parameters: $\mathcal{V}_{\text{SM}} = \mu^2 H^* H + \frac{1}{2}\lambda_1 H^* H^* HH$. Note that $\mu_{H\phi}$ is a critical parameter for the electromagnetic dipole moment operator (see Fig. 3) which, through Eq. (10), gets substituted by the VEV of ϕ^0. On the other hand, λ_5 is fundamental for the generation of neutrino masses, as can be seen from the diagram in Fig. 1, and its value is approximately proportional to the VEV of the S^0 scalar.

B. Neutrino masses

In the basis $(\nu, \Psi^0, \bar{\Psi}^0)^T$ the full mass matrix for neutral fermions reads, at tree level and in block form,

$$\mathcal{M}^0 = \begin{pmatrix} 0 & m_{Y_\Psi} & m_{Y_{\bar{\Psi}}}^T \\ m_{Y_\Psi}^T & 0 & M_\Psi \\ m_{Y_{\bar{\Psi}}} & M_\Psi^T & 0 \end{pmatrix}, \tag{11}$$

where $m_{Y_\Psi} = Y_\Psi v_H/\sqrt{2}$ and $m_{Y_{\bar{\Psi}}} = Y_{\bar{\Psi}} v_S/\sqrt{2}$. With the standard seesaw approximation, if the entries in the matrices $m_{Y_\Psi}(M_\Psi^{-1})^T$ and $m_{Y_{\bar{\Psi}}}(M_\Psi^{-1})^T$ are smaller than 1, one can block diagonalize $\mathcal{M}^0$ and the effective mass matrix for the light neutrinos is given by the expression

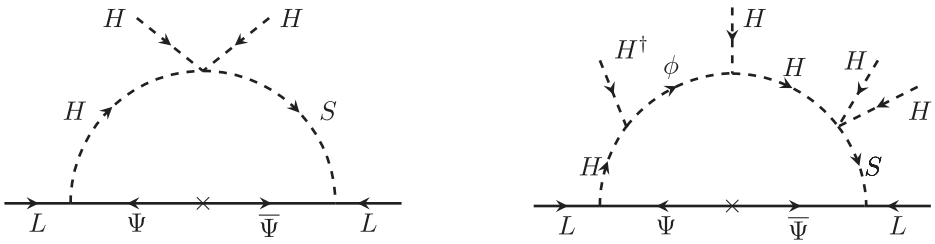

FIG. 4. Left: dimension-five diagram corresponding to the main one-loop neutrino mass contribution. Right: subleading dimension-seven neutrino mass contribution.

$$M_\nu = m_{Y_\Psi}(M_\Psi^{-1})^T m_{Y_\Psi} + m_{Y_\Psi}^T M_\Psi^{-1} m_{Y_\Psi}^T. \quad (12)$$

Note that, without loss of generality, the M_Ψ matrix can be taken to be diagonal.

If we take the neutrino mass diagram associated with this last formula (see Fig. 1) and close the outgoing Higgs H^* line with one of the ingoing Higgses H, we also obtain a radiative contribution to neutrino masses already in the original BNT model. In the basis where M_Ψ is diagonal, the correction to the tree-level formula can be expressed as

$$\Delta M_\nu^{\rm Loop} = \frac{1}{16\pi^2}(m_{Y_\Psi} M_{\rm Loop}^{-1} m_{Y_{\bar\Psi}} + m_{Y_{\bar\Psi}}^T M_{\rm Loop}^{-1} m_{Y_\Psi}^T), \quad (13)$$

where $M_{\rm Loop}^{-1}$ is a diagonal matrix with entries[3]

$$(M_{\rm Loop}^{-1})_{ii} \approx \frac{m_{\Psi_i}}{m_S^2 - m_h^2}\Delta B_0(m_S^2, m_h^2, m_{\Psi_i}^2) + \frac{m_{\Psi_i}}{m_S^2 - m_W^2}\Delta B_0(m_S^2, m_W^2, m_{\Psi_i}^2). \quad (14)$$

The quantity $\Delta B_0(m_A^2, m_B^2, m_{\Psi_i}^2) = B_0(0, m_A^2, m_{\Psi_i}^2) - B_0(0, m_B^2, m_{\Psi_i}^2)$ is related to the standard Passarino-Veltman function B_0. The main contribution to the radiative neutrino mass is shown in the left panel of Fig. 4. It should be noted that, with the introduction of the ϕ field, there is an extra loop contribution to neutrino masses (shown in the right panel of Fig. 4). Nevertheless, numerically its importance is small.

C. Scalar masses and mixing

In order to get a grasp on the magnitude and parameter dependence of the electromagnetic dipole moment operator in Eq. (3), it is important to understand how the various scalars mix. That discussion is simplified if we consider that the VEV of S is negligible ($v_S \approx 0$), in which case this field does not mix with the remaining ones. All scalar components of S can therefore be safely ignored (except in what concerns neutrino mass generation). However, we note that while this and other approximations made in the following discussion are very useful, to obtain the numerical results in Sec. III we used the full unapproximated expressions for masses and mixing angles.

We are left with three scalars with electric charge $+1$ contributing to the dipole moment operator, namely, H^+, ϕ^+, and $(\phi^-)^*$. For this particular ordering of the fields, their mass-squared matrix is given by the approximate expression

$$\mathcal{M}^+ \approx \begin{pmatrix} 2\frac{v_\phi^2}{v_H^2}(\kappa_1+\kappa_2) & \frac{\sqrt{2}v_\phi}{v_H}\kappa_1 & \frac{\sqrt{2}v_\phi}{v_H}\kappa_2 \\ \frac{\sqrt{2}v_\phi}{v_H}\kappa_1 & \kappa_3 & \kappa_1-\kappa_3 \\ \frac{\sqrt{2}v_\phi}{v_H}\kappa_2 & \kappa_1-\kappa_3 & -\kappa_1+\kappa_2+\kappa_3 \end{pmatrix}, \quad (15)$$

with

$$\kappa_1 \approx m_\phi^2 + 2\mu_\phi^2 + (\lambda_{6a}+\lambda_{6b}+2\lambda_9)\frac{v_H^2}{2}, \quad (16)$$

$$\kappa_2 \approx \kappa_1 - \lambda_{6b}\frac{v_H^2}{2}, \quad (17)$$

$$\kappa_3 \approx m_\phi^2 + (\lambda_{6a}+\lambda_{6b})\frac{v_H^2}{2}. \quad (18)$$

The properly normalized admixture of fields $v_H H^+ - \sqrt{2}v_\phi\phi^+ - \sqrt{2}v_\phi(\phi^-)^*$ constitutes the pseudo-Goldstone boson G^+, and therefore we are left with only two other mass eigenstates: φ_1^+ and φ_2^+. In order to make a quantitative analysis of their masses and composition, we shall take into account that v_ϕ must be significantly smaller than v_H, which in turn is much smaller than the bare masses m_ϕ^2 and μ_ϕ^2. When this is the case,

$$m^2(\varphi_1^+) \approx m_\phi^2 + 2\mu_\phi^2 + \left(\lambda_{6a} + \frac{1}{2}\lambda_{6b} + 2\lambda_9\right)\frac{v_H^2}{2}, \quad (19)$$

$$m^2(\varphi_2^+) \approx m_\phi^2 - 2\mu_\phi^2 + \left(\lambda_{6a} + \frac{1}{2}\lambda_{6b} - 2\lambda_9\right)\frac{v_H^2}{2}. \quad (20)$$

[3]To a good approximation, here we can use the value of the mass of S ignoring electroweak corrections.

There is also the following relation between electroweak and mass eigenstates:

$$\begin{pmatrix} G^+ \\ \varphi_1^+ \\ \varphi_2^+ \end{pmatrix} \approx \begin{pmatrix} 1 & -\sqrt{2}\frac{v_\phi}{v_H} & -\sqrt{2}\frac{v_\phi}{v_H} \\ 2\frac{v_\phi}{v_H} & \frac{1}{\sqrt{2}} & \frac{1}{\sqrt{2}} \\ 0 & -\frac{1}{\sqrt{2}} & \frac{1}{\sqrt{2}} \end{pmatrix} \begin{pmatrix} H^+ \\ \phi^+ \\ (\phi^-)^* \end{pmatrix}. \quad (21)$$

The neutral scalars, H^0 and ϕ^0, are equally important in the loop diagrams in Fig. 2. By splitting these two fields into their real and imaginary parts,

$$H^0 \equiv \frac{H_R^0 + iH_I^0}{\sqrt{2}}, \qquad \phi^0 \equiv \frac{\phi_R^0 + i\phi_I^0}{\sqrt{2}}, \quad (22)$$

it is easily seen that only the CP-even fields H_R^0 and ϕ_R^0 mix to form two mass eigenstates. One of them should be identified with the observed 125 GeV Higgs boson, and we will call the other one R^0. The CP-odd fields—H_I^0 and ϕ_I^0—do not mix, and hence they are mass eigenstates. In particular, $H_I^0 \equiv G^0$ is the neutral pseudo-Goldstone boson, just like in the SM. The expressions for the mass eigenstates are

$$h^0 \approx H_R^0 + 2\frac{v_\phi}{v_H}\phi_R^0, \quad R^0 \approx \phi_R^0 - 2\frac{v_\phi}{v_H}H_R^0, \quad G^0 = H_I^0, \quad \phi_I^0, \quad (23)$$

with the corresponding (pseudo)masses given by the following formulas:

$$m^2(h^0) \approx 4\lambda_1 v_H^2 - 4(m_\phi^2 + 2\mu_\phi^2)\frac{v_\phi^2}{v_H^2}, \quad m^2(R^0) \approx m^2(\varphi_1^+), \quad (24)$$

$$m^2(G^0) = 0, \qquad m^2(\phi_I^0) \approx m^2(\varphi_1^-). \quad (25)$$

D. Analytical understanding of the value of $(g-2)_{e,\mu}$ and related observables

With the approximate dependence of masses and mixing angles on the various Lagrangian parameters, we are in a position to estimate the value of $g-2$ for the electron and the muon, as well as the value of the lepton electric dipole moments and the branching ratios $\mathrm{Br}(\ell_\beta \to \ell_\alpha \gamma)$. Nevertheless, for our numerical results we used the full one-loop expressions, without approximations.

Following Ref. [22], we can describe a generic interaction of a fermion Ψ with the charged leptons $\ell_\alpha = e, \mu, \tau$ and a scalar Φ with couplings Γ_L^α and Γ_R^α:

$$\mathcal{L} = \cdots + \bar{\Psi}(\Gamma_L^\alpha P_L + \Gamma_R^\alpha P_R)\ell_\alpha \Phi^* + \mathrm{H.c.} \quad (26)$$

Through a loop diagram, this interaction will induce a contribution to the electromagnetic dipole moment operator shown in Eq. (3). Specifically, Ref. [22] quoted the result

$$c_R^{\alpha\beta} \approx \frac{1}{16\pi^2}\Gamma_L^{\alpha *}\Gamma_R^\beta \frac{m_\Psi}{m_\Phi^2}\left[f_\Phi\left(\frac{m_\Psi^2}{m_\Phi^2}\right) + q_\Psi g_\Phi\left(\frac{m_\Psi^2}{m_\Phi^2}\right)\right] \quad (27)$$

plus subleading contributions which are suppressed by the masses of the leptons ℓ_α and ℓ_β. The loop functions appearing in this expression are

$$f(x) = \frac{x^2 - 1 - 2x\log x}{4(x-1)^3}, \quad (28)$$

$$g(x) = \frac{x - 1 - \log x}{2(x-1)^2}, \quad (29)$$

and q_Ψ is the electric charge of the loop fermion, flowing from the initial lepton (ℓ_β) to the final one (ℓ_α).

The lepton anomalous magnetic moments, their electric dipole moments, as well as the branching ratios of the decays $\ell_\beta \to \ell_\alpha \gamma$ can readily be calculated from the numbers $c_R^{\alpha\beta}$:

$$\frac{(g-2)_\alpha}{2} \equiv a_\alpha = -4\frac{m_{\ell_\alpha}}{e}\mathrm{Re}c_R^{\alpha\alpha}, \quad (30)$$

$$d_\alpha = -2\mathrm{Im}c_R^{\alpha\alpha}, \quad (31)$$

$$\mathrm{Br}(\ell_\beta \to \ell_\alpha \gamma) = \frac{m_{\ell_\beta}^3}{4\pi\Gamma_{\ell_\beta}}(|c_R^{\alpha\beta}|^2 + |c_R^{\beta\alpha}|^2). \quad (32)$$

For the particular model under discussion, the main contribution to $c_R^{\alpha\beta}$ is due to the loop shown in Fig. 3. With the approximate value of the scalar mixing matrices provided earlier, we obtain the following estimate:

$$c_R^{\alpha\beta} \approx \frac{1}{16\pi^2}\sum_{i=1}^{3}(Y_\Psi)_{\alpha i}(Y_{e\phi} + Y_{e\phi^c})_{\beta i} m_{\Psi_i}\frac{v_\phi}{v_H} \times \sum_{\Phi=\{G^+,h^0,\varphi_1^+,R^0\}}\frac{\kappa_\Phi}{m_\Phi^2}\left[f\left(\frac{m_{\Psi_i}^2}{m_\Phi^2}\right) - \kappa'_\Phi g\left(\frac{m_{\Psi_i}^2}{m_\Phi^2}\right)\right]. \quad (33)$$

The $\kappa_\Phi^{(\prime)}$ coefficients in this expression take the following values: $\kappa_{G^+,h^0,\varphi_1^+,R^0} = (-\sqrt{2}, 1, \sqrt{2}, -1)$ and $\kappa'_{G^+,h^0,\varphi_1^+,R^0} = (2,1,2,1)$. At leading order, the remaining scalars do not contribute. Note also that the present model does not contain extra gauge bosons; however, the couplings of the SM ones to leptons is slightly altered. Instead of considering an extra loop with an internal $W^\pm$ boson, it is sufficient to include in the scalar computation the

pseudo-Goldstone boson G^+, assigning to it its physical mass ($m_{G^+} = m_W$).

III. RESULTS AND DISCUSSION

In this section we will discuss the numerical results for $\Delta(g-2)_\alpha$ ($\alpha = e, \mu$), the neutrino mass fits, and constraints from charged lepton-flavor-violation (cLFV) searches. We also briefly comment on electric dipole moments $d_{e,\mu}$. The discussion is divided into two parts. In the first one we show results for the original BNT model, while in the second we discuss the extended version, BNTϕ.

We have implemented the model into SARAH [40,41]. This program generates SPheno routines [42,43] for a numerical calculation of mass spectra and other observables. To cross-check the results, we have written private codes for the numerical evaluation of $\Delta(g-2)_\alpha$ and also implemented the approximation formulas discussed in Sec. II.

A. Results for the BNT model

Since the main motivation for the BNT model [39] is to explain the observed neutrino oscillation data, we first briefly discuss how neutrino masses and angles can be fitted to the experimental data.

The master parametrization [44,45] allows us to fit any Majorana neutrino mass model to experimental data. For the case of the BNT model, the general formulas in Ref. [45] simplify to

$$Y_1 = cM_\Psi^{1/2} W T \hat{m}_\nu^{1/2} U_\nu^\dagger,$$
$$Y_2 = cM_\Psi^{1/2} W^* B \hat{m}_\nu^{1/2} U_\nu^\dagger, \tag{34}$$

with

$$B = (T^T)^{-1}(\mathbb{I} - K), \tag{35}$$

and $c = (v_H v_S)^{-1/2}$. Since the neutrino mass matrix is symmetric under the exchange of Y_1 and Y_2, we can associate Y_Ψ and $Y_{\bar{\Psi}}$ with either of them arbitrarily. The master parametrization calculates the two Yukawa matrices as functions of the input parameters m_{ν_i}, U_ν, and M_Ψ and three matrices W, T, and K with arbitrary parameters. Here, W is a unitary matrix, T is an upper triangular matrix, and K is an antisymmetric matrix. All matrices are (3, 3). As usual, $\hat{m}_\nu$ and U_ν are the light neutrino mass eigenvalues and mixing matrix.[4]

An especially simple case is the choice $W = \mathbb{I}$, $T = f \times \mathbb{I}$, and $K = 0$. This leads to $Y_\Psi = f^2 Y_{\bar{\Psi}}^T$ and both Yukawa matrices are equal for $f = 1$. With this choice, both Yukawa matrices have off-diagonal elements due to the large mixing angles observed in oscillation experiments. Figure 5 shows $\Delta(g-2)_\alpha$ and $\mathrm{Br}(l_i \to l_j \gamma)$ for some fixed masses m_{Ψ_i} as functions of the diagonal entries in Y_Ψ, $|(Y_\Psi)_{ii}|$. Since the neutrino fit requires the product of the two Yukawa matrices to be constant, small values of $|(Y_\Psi)_{ii}|$ correspond to large entries in $Y_{\bar{\Psi}}$ and vice versa.

As the plots in Fig. 5 show, $\Delta(g-2)_\mu$ can be explained if either $|(Y_\Psi)_{22}|$ or $|(Y_{\bar{\Psi}})_{22}|$ are order $\mathcal{O}(1)$.[5] However, $\Delta(g-2)_e$ is always smaller than the experimental anomaly.[6] Even more importantly, cLFV constraints [especially $\mathrm{Br}(\mu \to e\gamma)$] rule out all points that explain $\Delta(g-2)_\mu$ in this fit.

We have therefore tried a different ansatz for the matrices W and T. It is easy to show that the choice $W = U_\nu$ and $T = f \times \hat{m}_\nu^{-1/2}$ will lead to a fit of neutrino data in which one of the two Yukawa matrices is diagonal. Figure 6 shows the result of this calculation. Here we show $\Delta(g-2)_\mu$ for two choices of m_Ψ. Full lines are for $m_\Psi = 800$ GeV, while dashed lines are for $m_\Psi = 1.5$ TeV. These values are motivated by the (estimated) lower limit and future sensitivity of the LHC; see the discussion in Sec. IV. Colored points are allowed by cLFV constraints, while points violating the experimental bound on $\mathrm{Br}(\mu \to e\gamma)$ are shown in grey. The plot in the left panel fits neutrino data with a diagonal matrix Y_Ψ, while the plot in the right panel is for diagonal $Y_{\bar{\Psi}}$. As expected, the model can explain $\Delta(g-2)_\mu$, consistent with the bound on $\mathrm{Br}(\mu \to e\gamma)$, if the larger of the two Yukawa matrices is diagonal. The plots show that both $\hat{Y}_\Psi$ and $\hat{Y}_{\bar{\Psi}}$ give valid solutions. Again, $\Delta(g-2)_e$ is never large enough to explain the experimental anomaly.

While the BNT model can explain $\Delta(g-2)_\mu$, at least one of the Yukawas needs to be $\mathcal{O}(1)$, given current lower limits on the heavy fermion masses. In fact, as we show in Fig. 7, in the BNT model one can derive an upper bound on the mass of Ψ from the requirement that the experimental anomaly is correctly explained. As Fig. 7 demonstrates, even for $|(Y_\Psi)_{22}| = 4\pi$, m_Ψ cannot be larger than roughly 3 TeV in this case. Note that such a large coupling makes

[4] An alternative but equivalent fit could be done using one of the two Yukawa couplings as input:

$$Y_\Psi = \left(\frac{1}{v_H v_S} M_\nu + A\right)(Y_{\bar{\Psi}})^{-1} M_\Psi, \tag{36}$$

with A being a generic antisymmetric matrix and M_ν the neutrino mass matrix in the flavor basis.

[5] The plots in Figs. 5 and 6 are shown versus $(Y_\Psi)_{11}$. Since we fit neutrino data using Eq. (34) for fixed, best-fit-point neutrino data, the ratios of all different entries in the Yukawa matrix are constant in this scan. For example, $(Y_\Psi)_{22}/(Y_\Psi)_{11} \simeq 6$ at all points in these plots.

[6] Since we plot logarithmically, the plot shows $|\Delta(g-2)_e|$. Experimentally, $\Delta(g-2)_\mu$ and $\Delta(g-2)_e$ have different signs. We have checked that the relative signs can be easily generated by relative signs in the entries of the Yukawa matrices.

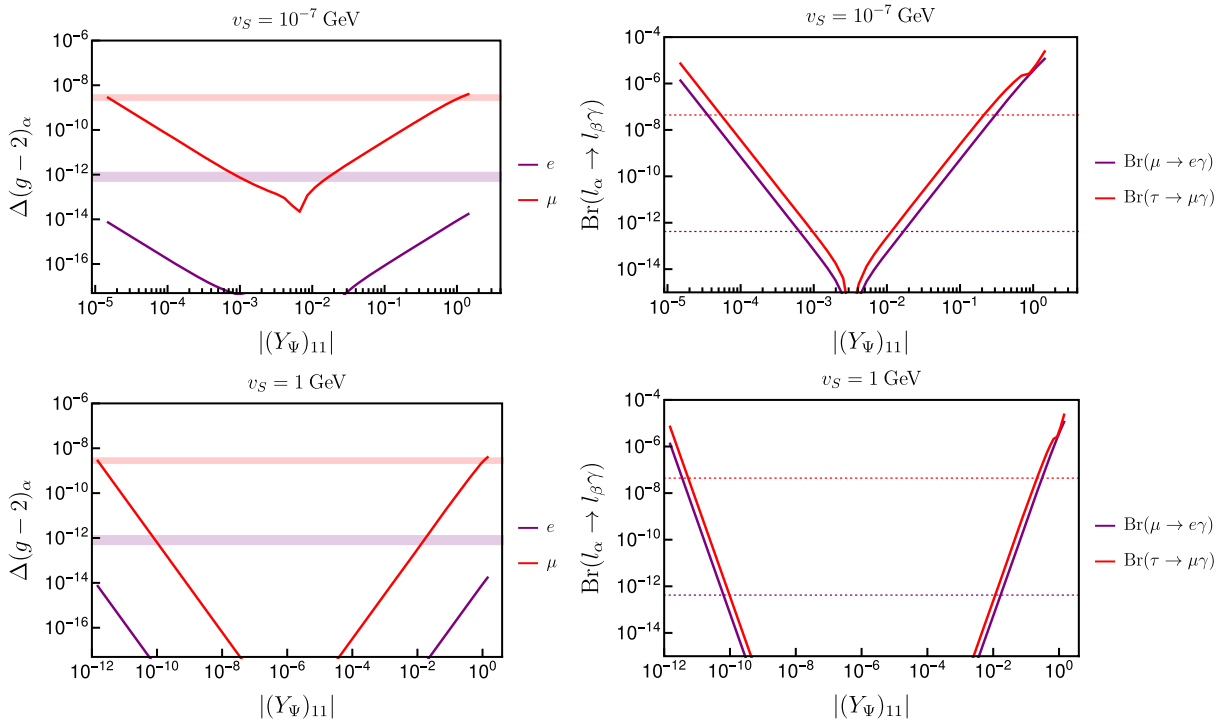

FIG. 5. Left: $\Delta(g-2)_\alpha$, the shift with respect to the SM value of $(g-2)_\alpha$, as a function of $|(Y_\Psi)_{11}|$ for two choices of the quadruplet VEV, v_S. We only show $\alpha = e, \mu$, since there is practically no experimental information for the τ. The thin horizontal bands are the 1σ C.L. ranges of the experimental anomalies. Right: $\mathrm{Br}(l_i \to l_j\gamma)$ for the same choice of parameters as in the left panels. The masses of Ψ_i are chosen as $m_{\Psi_{1,2,3}} = (0.8, 0.9, 1.0)$ TeV, and the mass of the scalar quadruplet is $m_S = 500$ GeV. For the neutrino fit, see the discussion in the text.

the model nonperturbative, and thus this number is conservative and the LHC should be able to test values up to $|(Y_\Psi)_{22}| \sim$ (6–7).

B. Results for the BNTϕ model

Let us turn now to a discussion of the extended BNT model. The addition of the scalar ϕ to the model generates diagrams, for which the mass flip [necessary for the generation of $\Delta(g-2)_\alpha$] can be caused by the large fermion mass internal to the loop.

Figure 8 shows a comparison of the approximation formulas (see Sec. II) to the full numerical results from SPheno. The plot shows $\Delta(g-2)_\alpha$ as a function of m_ϕ for different values of v_ϕ and $Y_{e\phi} = Y_{e\phi^c}$. The neutrino fit was

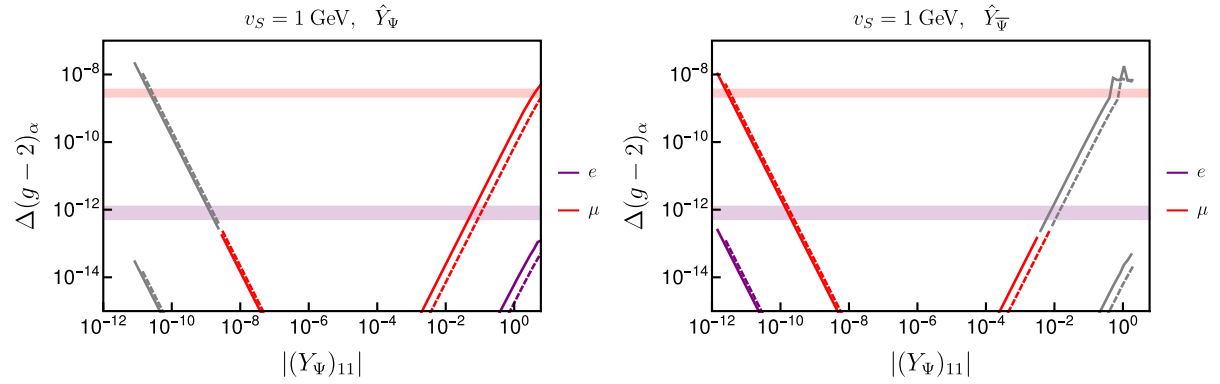

FIG. 6. $\Delta(g-2)_\alpha$ as a function of $|(Y_\Psi)_{11}|$. m_{Ψ_i} are chosen as $m_{\Psi_{1,2,3}} = (0.8, 0.9, 1.0)$ TeV (solid lines) and $m_{\Psi_{1,2,3}} = (1.5, 1.6, 1.7)$ TeV (dashed lines). Grey points are ruled out by the experimental limit on $\mathrm{Br}(\mu \to e\gamma)$. For the neutrino fit, see the discussion in the text.

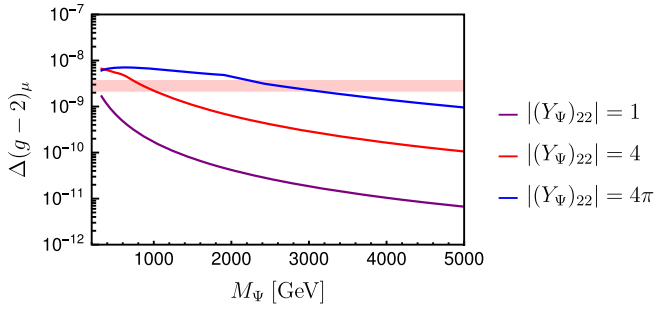

FIG. 7. $\Delta(g-2)_\mu$ for three fixed values of $(Y_\Psi)_{22}$ as a function of M_Ψ, for degenerate Ψ.

done with a diagonal coupling Y_Ψ, with entries on the diagonal equal to $(Y_\Psi)_{ii} = 1$ for simplicity. The plots demonstrate that there is a large range of parameter space for which both experimental anomalies can be explained simultaneously. It may seem counterintuitive that $\Delta(g-2)_\alpha$ increases with increasing mass m_ϕ. The reason for this is the relative sign between the diagrams from the Goldstones and the scalars; see Eq. (33). This sign leads to a cancellation in $\Delta(g-2)_\alpha$ if the scalars h^0 and ϕ^+ are degenerate with the corresponding Goldstone bosons. For large m_ϕ this cancellation is less effective, and in the limit $m_\phi \to \infty$ only the Goldstone diagrams contribute to the observable.

Figure 8 also demonstrates that the approximation formulas work quite well for a v_ϕ of order $\mathcal{O}(\text{GeV})$, as expected. For the muon, the approximation formula starts to differ from the numerical results once v_ϕ and $Y_{e\phi}$ are smaller than a GeV and $Y_{e\phi} \ll 1$, respectively, while for the electron the approximation still works reasonably well. Again, this is to be expected because, since $m_\mu/m_e \simeq 200$, diagrams with external mass flips are more important in the case of the muon. Depending on other model parameters, the diagrams proportional to v_ϕ will be subdominant even for very large (i.e., nonperturbative) Yukawa couplings for $v_\phi \lesssim (10^{-3}\text{–}10^{-2})$ GeV. For v_ϕ below 10^{-3} GeV the model cannot explain $\Delta(g-2)_e$ and the results of the original BNT model are approximately recovered.

Since roughly $\Delta(g-2)_\alpha \propto 1/m_\Psi$, correctly explaining the experimental anomalies would imply an upper limit on m_Ψ. The most conservative value for this limit is reached if all Yukawa couplings take the maximum values allowed by perturbativity. Taking $\forall\, Y \sim (4\pi)$, the result is roughly of order $m_\Psi \sim \mathcal{O}(100)$ TeV. This number is so large that it is only of academic interest. Figure 9 shows that for large m_ϕ (say, m_ϕ larger than 1 TeV) there is practically no dependence on the choice of m_ϕ. The reason for this is that in this limit all of the heavy scalar states decouple from the calculation and the only contribution to the observable comes from the Goldstone diagrams.

Figure 9 also demonstrates that for more reasonable couplings the upper limit on m_Ψ is again much lower. Allowing $Y_{e\phi} = 4\pi$ but restricting Y_Ψ to order $\mathcal{O}(1)$, the limit is roughly (8–10) TeV, while for all couplings no larger than 1 one finds $m_\Psi \leq$ (2–3) TeV. This last number is close to what the LHC can probe in the high-luminosity run, although the LHC will not be able to cover the allowed range of masses completely; see the next section.

Let us briefly discuss the electric dipole moments d_α. Figure 10 shows one example as a function of m_Ψ. The couplings $Y_{e\phi}$ and $Y_{e\phi^c}$ have been taken to be real and equal to one, $Y_{e\phi} = Y_{e\phi^c} = 1$. The plot shows that d_e provides a severe constraint, while for d_μ there is no part of the parameter space where the model can saturate the experimental bound. The plot uses the same parameters and fitting as that used in Fig. 9 for $\Delta(g-2)_\alpha$. d_e probes phases as low as 10^{-6}. Thus, the large couplings needed to explain $\Delta(g-2)_e$ essentially need to be real.

For the BNTϕ model, in order to generate the CP phase δ in the neutrino fit, one can always put the phases into the

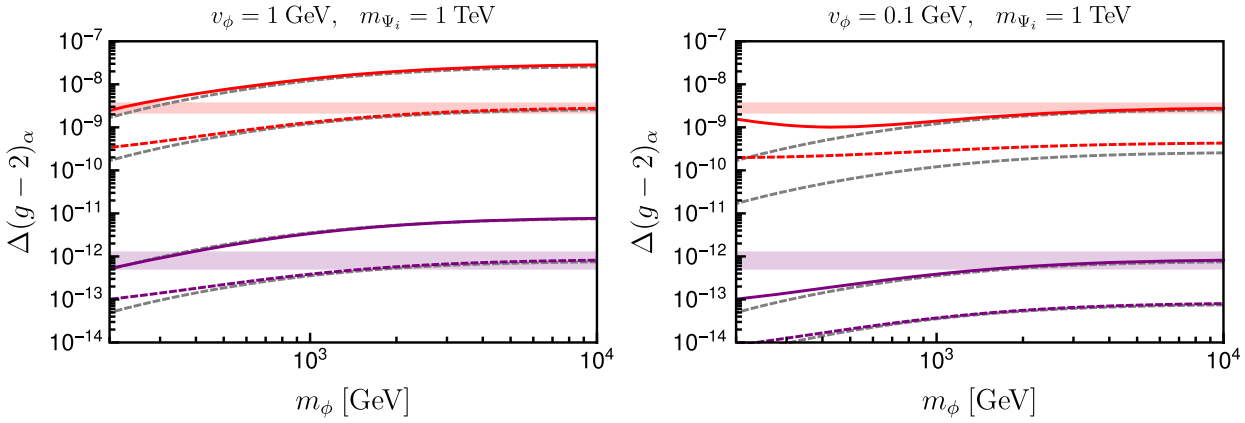

FIG. 8. $\Delta(g-2)_\alpha$ as a function of m_ϕ for different values of v_ϕ and $Y_{e\phi} = Y_{e\phi^c}$. The colored lines are the numerical result, while the gray lines are calculated with the approximation formulas (see text). Full lines are calculated with $(Y_{e\phi})_{11} = 0.06$ and $(Y_{e\phi})_{22} = 1$, while dashed lines are with $(Y_{e\phi})_{11} = 0.006$ and $(Y_{e\phi})_{22} = 0.1$. As in all other figures in this section, red is for μ and purple is for e.

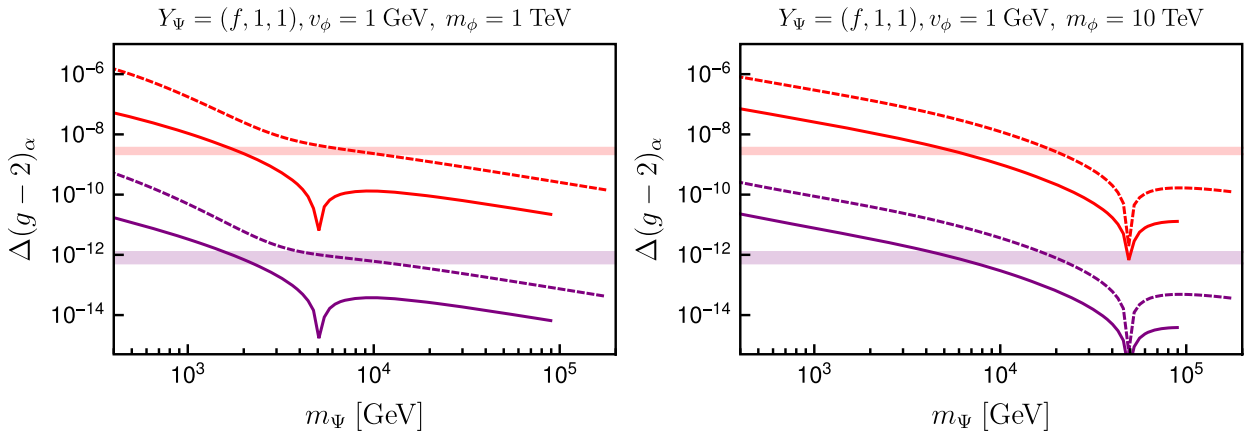

FIG. 9. $\Delta(g-2)_\alpha$, the shift with respect to the SM value of $(g-2)_\alpha$, as a function of m_Ψ. The mass of the scalar ϕ is $m_\phi = 1$ TeV (left) and $m_\phi = 10$ TeV (right). The neutrino data is fitted with a diagonal Y_Ψ and the factor f has been chosen as $f \simeq 0.06$ to fit the two experimental anomalies at the same value of m_Ψ. This is neither necessary nor a prediction of the model and has been done only for demonstration. The points have been calculated assuming $Y_{e\phi} = Y_{e\phi^c}$, and the solid lines are for $(Y_{e\phi})_{ii} = 1$ while the dashed lines are for $(Y_{e\phi})_{ii} = 4\pi$.

small Yukawa coupling. (In the case of Fig. 10 we use $Y_{\bar{\Psi}}$). Thus, the model can survive the d_e constraint easily, but it also does not make any testable predictions.

The large couplings have to be both real and close to diagonal, as Fig. 11 demonstrates. Here, Y_Ψ has simply been parametrized as

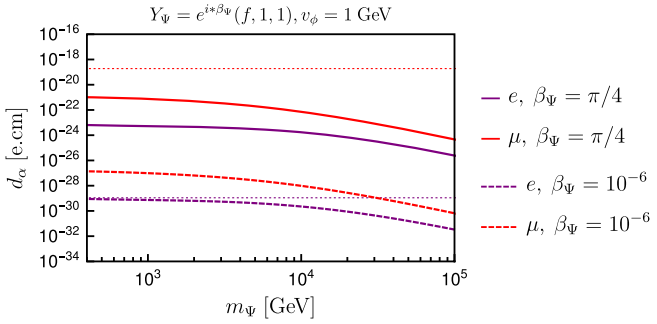

FIG. 10. d_α, the electric dipole moments, as a function of m_Ψ. The large couplings, except $(Y_\Psi)_{11}$, have all been taken to be equal to 1 in this plot.

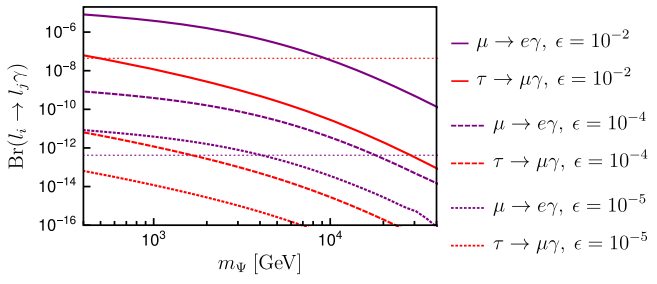

FIG. 11. $\mathrm{Br}(l_i \to l_j\gamma)$ as a function of m_Ψ. The large couplings have all been taken to be equal to 1 in this plot. For the parametrization of Y_Ψ, see the main text.

$$Y_\Psi = \begin{pmatrix} f & \epsilon & \epsilon \\ \epsilon & 1 & \epsilon \\ \epsilon & \epsilon & 1 \end{pmatrix}. \tag{37}$$

Here, $f \simeq 0.06$, as discussed above. $\mu \to e\gamma$ provides a severe constraint on the off diagonal in the (12) sector: $\epsilon \leq 10^{-(5/6)}$, depending on the mass of Ψ. $\tau \to \mu\gamma$ is much less stringent, but still provides $\epsilon \leq 10^{-2}$ for the lowest m_Ψ.

In summary, the extended version of the BNT model, BNTϕ, can simultaneously explain the experimentally observed anomalies in $(g-2)$ and easily fit neutrino oscillation data in large parts of its parameter space. Electric dipole moments force the large Yukawa coupling required for $\Delta(g-2)_\alpha^{\mathrm{exp}}$ to be (nearly) real, while cLFV constraints require them to be (nearly) diagonal. This has some interesting consequences for the phenomenology of the heavy fermions Ψ, as we discuss in the next section.

IV. HEAVY FERMIONS AT COLLIDERS

We calculated the production cross sections for the different heavy fermions of the BNT model using MADGRAPH [46–48]. For the pair production of multiply charged particles, photon-photon fusion diagrams are especially important at large scalar masses, despite the tiny parton density of the photon inside the proton. Manohar *et al.* [49,50] recently reported an updated determination of the photon parton distribution function (PDF) inside the proton. The resulting `LUXqed17_plus_PDF4LHC15_nnlo_100` combines QCD partons from `PDF4LHC15` [51] with the LUXqed calculation of the photon density. Results for cross sections using this set of PDFs are shown in Fig. 12 for the LHC and a hypothetical future 100 TeV pp collider.

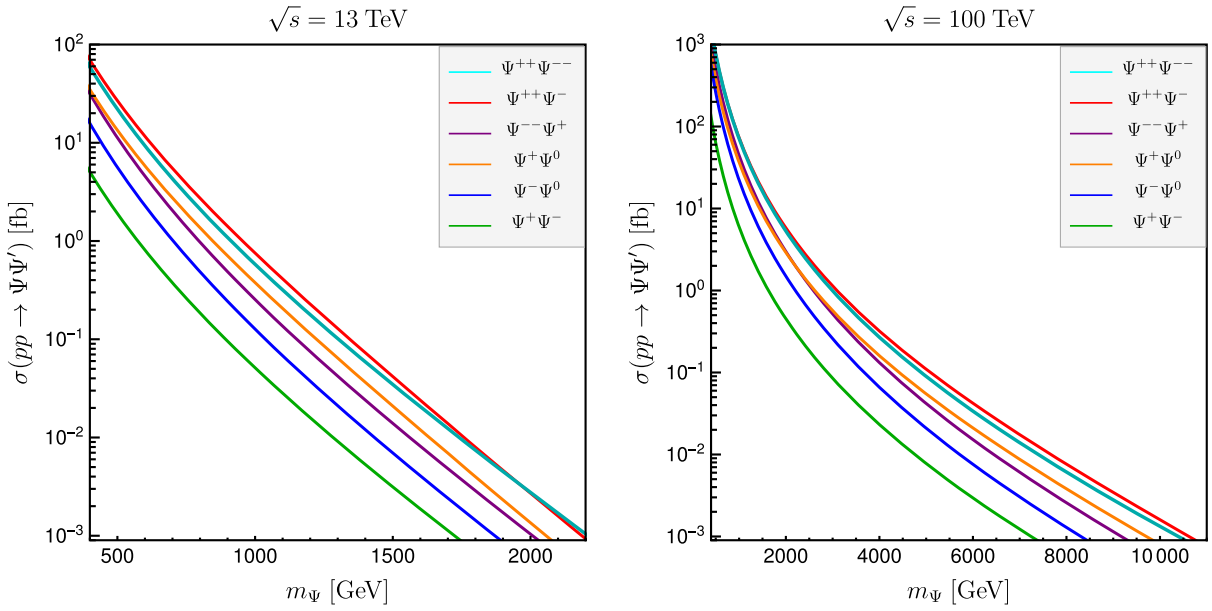

FIG. 12. Production cross sections for the exotic fermions in the BNT model for the LHC (left) and a future 100 TeV collider (right).

The largest cross sections are the pair production of the doubly charged fermions and the associated production of $\Psi^{++}\Psi^{-}$. For the high-luminosity LHC with $\mathcal{L} = 3/\text{ab}$ each of these gives more than 100 (20) events for $m_\Psi = 1.5$ (1.8) TeV before cuts. Therefore, we expect that, depending on search strategy and backgrounds, the final reach of the LHC for the discovery of the heavy fermions of the BNT model should roughly lie in this mass range.

Possible decays of the heavy fermions depend on whether the scalars S and/or ϕ are lighter or heavier than Ψ. We will concentrate on the case that all new scalars are heavier than the fermions for definiteness. Final states for the different Ψ are $\Psi_i^{++} \to l_j^+ W^+$, $\Psi_i^+ \to (l_j^+ Z^0, l_j^+ h^0, \nu_j + W^+)$, and $\Psi_i^0 \to (l_j^\pm + W^\mp, \nu_j + h^0, \nu_j + Z^0)$. Since Ψ_i^0 are Majorana fermions, both lepton charges should occur with (nearly[7]) equal branching ratios.

Before entering into a more detailed discussion of the different branching ratios, let us comment briefly on existing limits from LHC searches. Several "exotic" searches at ATLAS and CMS can provide lower mass limits on Ψ. The currently most stringent one is, to our knowledge, the multilepton search by CMS [52]. This work uses a total of 137/fb of statistics to search for three charged leptons with missing energy in the final state and no hadronic activity associated with the events. The target process is the type-III seesaw, and the final state searched for can be generated in this model via $pp \to \Sigma^+\Sigma^0 \to (W^+\nu) + (W^+ l^-) \to l^+ l^+ l^- \nu\nu$, from the leptonic decays of the W's. For Σ decaying "flavor democratically" the lower limit is $m_\Sigma = 880$ GeV. (This assumes equal branching ratios to the different lepton families. For Σ decaying to τ's the limit is considerably worse; see Ref. [52] and for more details the earlier Ref. [53]). While both cross sections and branching ratios are different in the seesaw type-III and the BNT model, a rough estimate using Fig. 11 of Ref. [52] gives a lower limit on m_Ψ in the range of (800–900) GeV for Ψ^{++} decaying to e or μ.

Let us now turn to a discussion of the decay branching ratios of the heavy fermions. As discussed in the previous section, neutrino data requires that at least one of the matrices Y_Ψ or $Y_{\bar{\Psi}}$ be nondiagonal. Since the same couplings are responsible for the decays of the heavy fermions, in general one would expect the decays of Ψ^{++}, Ψ^+, and Ψ^0 to also violate flavor.

An example is shown in Fig. 13. Here we show the total decay width of Ψ^{++} and $\text{Br}(\mu \to e\gamma)$ (left panels) as well as the branching ratios $\text{Br}(\Psi^{++} \to l_j^+ W^+)$ for $j = e, \mu, \tau$ (right panel) as a function of v_S. For this figure we have chosen $m_{\Psi_1} = 1$ TeV and the neutrino masses were fitted with Eq. (34). In this scan we randomly choose the angles in matrix W, we restrict the entries in the matrix T to be order $\mathcal{O}(1)$ on the diagonal and $\mathcal{O}(10^{-1})$ on the off diagonal, and for simplicity $K \equiv 0$. Note that, due to the restrictions on T, Y_Ψ and $Y_{\bar{\Psi}}$ have a similar order of magnitude in this plot. The plot in the left panel shows that both $\text{Br}(\mu \to e\gamma)$ and the total width of Ψ^{++} decrease with increasing v_S, since a larger v_S requires smaller Yukawa couplings in the neutrino fit. The plot in the right panel, however, shows no such tendency in the branching ratios. This is easily understood: while the total width is sensitive to the overall size of the Yukawa couplings, ratios of branching ratios depend only

[7] CP-violating phases can lead to small differences in the branching ratios to leptons or antileptons. We do not address these details, since the lepton asymmetry caused by this difference is a one-loop correction to the branching ratio.

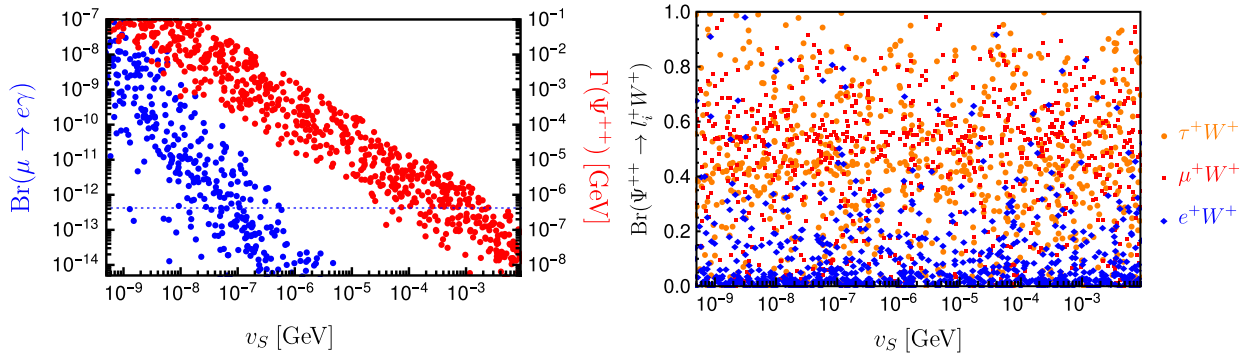

FIG. 13. Left: total width of Ψ^{++} and $\mathrm{Br}(\mu \to e\gamma)$ as a function of v_S. Right: branching ratios of Ψ^{++}. The plot shows a random scan for a fixed mass $m_\Psi = 1$ TeV (see text).

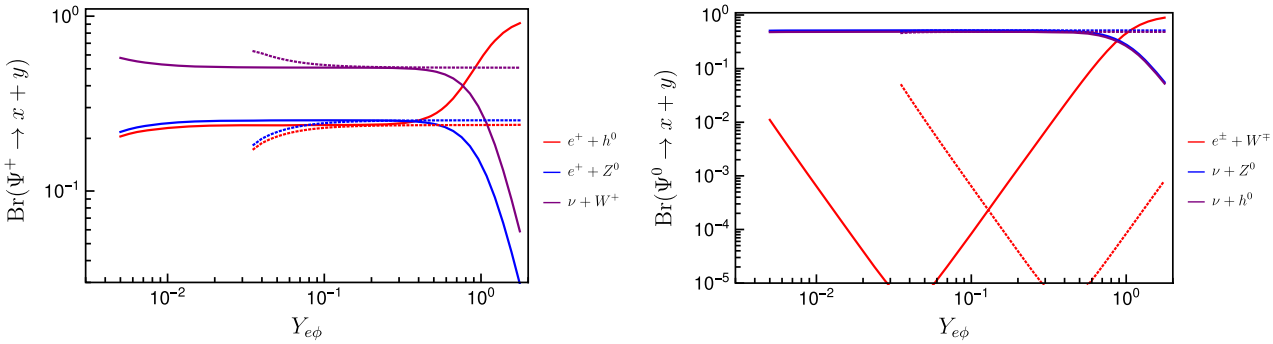

FIG. 14. Branching ratios for the decays of Ψ_1^+ and Ψ_1^0 as a function of $Y_{e\phi}$, for two different values of v_ϕ, $v_\phi = 1$ GeV (0.1 GeV), shown by the solid lines (dashed lines). All points in this plot are within the 1σ C.L. range of the two experimental anomalies, $\Delta(g-2)_e$ and $\Delta(g-2)_\mu$. This is achieved by fitting Y_Ψ as a function of $Y_{e\phi}$. In this case, all decays are flavor diagonal, as discussed in the text.

on ratios of Yukawa couplings. Thus, an upper limit on $\mathrm{Br}(\mu \to e\gamma)$ does not restrict the possibility to have flavor-violating Ψ^{++} decays.[8] Results for the decays of Ψ^+ and Ψ^0 show the same qualitative behavior, and we do not repeat these plots here.

The situation is very different in those parts of parameter space where the model can explain $\Delta(g-2)_e$ and obey the upper bound from cLFV decays at the same time. As discussed in the previous section, Y_Ψ (or $Y_{\tilde{\Psi}}$) and $Y_{e\phi}$ must be "large" and nearly diagonal to fit $\Delta(g-2)_e$. In this case all heavy fermion decays are very nearly flavor diagonal. We have numerically checked that points with Y_Ψ and $Y_{e\phi}$ in the range that gives the correct $\Delta(g-2)_e$ cannot have measurable flavor-violating decays of the heavy fermions without grossly violating existing cLFV bounds.

Moreover, the decays of Ψ_1^+ and Ψ_1^0 depend on the values of v_ϕ and $Y_{e\phi}$. Figure 14 shows an example. In these plots branching ratios are shown as a function of $Y_{e\phi}$ for two values of v_ϕ. All points in this plot are within the 1σ C.L. range of the two experimental anomalies, $\Delta(g-2)_e$ and $\Delta(g-2)_\mu$. For values of $v_\phi < (\text{few})10^{-3}$ GeV, $\Delta(g-2)_e$ cannot be fitted anymore with perturbative Yukawa couplings. The lines stop on the left side, when Y_Ψ becomes nonperturbative. Note that Y_Ψ is fitted to the experimental data as a function of $Y_{e\phi}$, and thus $Y_\Psi \gg Y_{\tilde{\Psi}}$ in this calculation.

It is interesting to point out that for $Y_{e\phi} \gg Y_\Psi$, which occurs only for $v_\phi = 1$ GeV in these figures, the decays $\Psi^+ \to e^+ h^0$ and $\Psi^0 \to e^\pm W^\mp$ are enhanced. This particular pattern appears only in the BNTϕ model (and not in the original BNT model). One can trace it back analytically to the appearance of the coupling $Y_{e\phi}$ in the coupling of the heavy fermions to the SM Higgs, due to the mixing of H and ϕ (proportional to v_ϕ/v).

We note that the model does not predict the hierarchy among the different copies of Ψ. Thus, the lightest of these can couple dominantly to either e, μ, or τ. Figure 14 shows the case where the lightest Ψ couples to e. The plots for the other cases (coupling to μ or τ) are very similar and we do not repeat them here.

[8]For flavor violation in heavy fermion decays one must consider the full event. For example, the pair production of $\Psi^{++}\Psi^{--}$ leads to $l_i^+ l_j^- + 4j$ (from hadronic W decays), with $i \neq j$, if Ψ^{++} decays to more than one lepton generation.

In summary, the heavy fermions Ψ of the BNT model can be produced at the high-luminosity LHC. While in general one expects to have large LFV decays of the heavy fermions, fitting $\Delta(g-2)_e$ to the experimental anomaly requires large and flavor-diagonal couplings. Thus, in order for the model to explain $\Delta(g-2)_e$, the heavy fermions must decay in a flavor-conserving manner. Interestingly, the decays of Ψ^+ and Ψ^0 also indirectly trace the presence of ϕ in the model via enhanced rates for the decays $\Psi^+ \to e^+ h^0$ and $\Psi^0 \to e^\pm W^\mp$, if $Y_{e\phi}$ is the largest Yukawa coupling.

V. SUMMARY

We proposed an extension of the original BNT neutrino model to accommodate the experimental $(g-2)_\alpha$ ($\alpha = e, \mu$) anomalies, compatible with neutrino oscillation data and current cLFV bounds. In this model, the presence of an extra hypercharge-zero triplet scalar gives a sizable contribution to the dipole operator proportional to the mass of the exotic heavy fermions. The situation is different for the original BNT model, where the dipole operators are suppressed by the small charged lepton masses. Consequently, the original BNT model cannot explain both anomalies at the same time, but $\Delta(g-2)_\mu$ could be explained if at least one of the exotic fermions has a mass of roughly $m_\Psi \lesssim (2\text{–}3)$ TeV, which is partially within reach of the high-luminosity LHC.

In the extended BNT model an explanation of both observed anomalies, $(g-2)_e$ and $(g-2)_\mu$, is compatible with neutrino oscillation data and perturbative couplings in a large part of the available parameter space. The smallness of the observed m_ν, together with the requirement to correctly explain the $(g-2)$ anomalies, selects a specific part of the parameter space. Specifically, $Y_{e\phi}$ and either Y_Ψ or $Y_{\bar{\Psi}}$ have to be order $\mathcal{O}(0.1\text{–}1)$. cLFV bounds then force the large couplings to be (nearly) flavor diagonal. Additional constraints on these couplings come from the current EDM bounds of the electron. We showed that the experimental bound for $|d_e| \sim 1.1 \times 10^{-9}\ e\,\mathrm{cm}$ forces the large couplings needed to explain $\Delta(g-2)_e$ to be mostly real. These results are in agreement with model-independent considerations which can be made based on an effective field theory analysis [22]. For d_μ, on the other hand, the model cannot give large enough values to saturate the current experimental bound. No observation of d_μ is therefore expected in the current model.

Since current cLFV bounds require the large couplings to be nearly diagonal in order to avoid large cLFV observables, decays of the heavy fermions are necessarily flavor conserving. We discussed the decays of $(\Psi^0, \Psi^+, \Psi^{++})$ for the case that the scalars are heavier than the fermions. We used MADGRAPH [46–48] together with the LUXqed PDFs [49,50] to calculate production cross sections of the different heavy fermions for the LHC and a possible future $\sqrt{s} = 100$ TeV hadron collider. For the high-luminosity LHC, future searches for the heavy fermions of the BNT model can probe masses up to roughly $m_\Psi \leq (1.5\text{–}1.8)$ TeV.

We discussed branching ratios of the heavy fermions. Ψ_α^{++} decay via $\Psi_\alpha^{++} \to l_\alpha^+ W^+$ with 100%, whereas $\Psi_\alpha^+ \to (l_\alpha^+ h^0, l_\alpha^+ Z^0, \nu W^+)$. The branching ratio to $l_\alpha^+ h^0$ is enhanced if $Y_{e\phi} \gtrsim \mathcal{O}(1)$. Similarly, for Ψ^0 decays the branching ratios $\Psi_\alpha^0 \to l_\alpha^\pm W^\pm$ can be large in the same parts of parameter space. In summary, the extended BNTϕ model can explain the observed anomalies in $(g-2)$, while making interesting predictions for the decay patterns of the exotic fermions.

ACKNOWLEDGMENTS

This work is supported by the Spanish grants FPA2017-85216-P (MINECO/AEI/FEDER, UE) and PROMETEO/2018/165 grants (Generalitat Valenciana). R. C. is also supported by FPU15/03158 (MICINN). R. F. acknowledges the financial support from the Grant Agency of the Czech Republic (GAČR) through contract number 20-17490S and from the Charles University Research Center UNCE/SCI/013. C. A. is supported by FONDECYT-Chile Grant No. 11180722 and ANID-Chile PIA/APOYO AFB 180002.

APPENDIX: FULL LAGRANGIAN EXPRESSION

The full expression of the extra interactions and mass terms of the BNTϕ model, including $SU(2)_L$ indices $(i, j, \ldots, p)$, is as follows.

$$\begin{aligned}\mathcal{L}_{\mathrm{BNT}\phi} = {} & M_\Psi \Psi_{ij} \bar{\Psi}_{ij} + Y_\Psi L_i \Psi_{ji} H_j^* + Y_{\bar{\Psi}} \bar{\Psi}_{lj} L_m S_{ijk} \epsilon_{im} \epsilon_{kl} + Y_{e\phi} e^c \bar{\Psi}_{ij} \phi_{ji} \\ & + Y_{e\phi^c} e^c \bar{\Psi}_{ij} \phi_{ij}^* + Y_{\Psi\phi} \Psi_{ij} \bar{\Psi}_{jk} \phi_{ki} + Y_{\Psi\phi^c} \Psi_{ij} \bar{\Psi}_{jk} \phi_{ik}^* - \mathcal{V}, \end{aligned} \tag{A1}$$

$$\begin{aligned}\mathcal{V} = {} & m_S^2 S_{ijk}^* S_{ijk} + m_\phi^2 \mathrm{Tr}(\phi^\dagger\phi) + [\mu_\phi^2 \mathrm{Tr}(\phi\phi) + \mathrm{H.c.}] + [\mu_{H\phi} H^\dagger \phi H \mu_{S\phi} S_{ijk}^* S_{ijl} \phi_{kl} + \mathrm{H.c.}] \\ & + \frac{1}{2}\lambda_{2a}(S_{ijk}^* S_{ijk})^2 + \frac{1}{2}\lambda_{2b} S_{ijk}^* S_{mno}^* S_{ljk} S_{pno} \epsilon_{im}\epsilon_{lp} \frac{1}{2}\lambda_3 (H^\dagger H) S_{ijk}^* S_{ijk} \\ & + \frac{1}{2}\lambda_4 H_j H_i^* S_{klm}^* S_{nlm} \epsilon_{ik}\epsilon_{jn} + \lambda_{6a}(H^\dagger H)\mathrm{Tr}(\phi^\dagger\phi)\lambda_{6b} H^\dagger \phi\phi^\dagger H + \lambda_{7a}(S_{ijk}^* S_{ijk})\mathrm{Tr}(\phi^\dagger\phi) \\ & + \lambda_{7b} S_{ijk}^* S_{ijn} (\phi\phi^\dagger)_{kn} \lambda_{7c} S_{ijk}^* S_{ilm} (\epsilon\phi^*)_{jk} (\epsilon\phi)_{lm} + \lambda_{8a}[\mathrm{Tr}(\phi^\dagger\phi)]^2 \\ & + \lambda_{8b}\mathrm{Tr}(\phi\phi\phi^\dagger\phi^\dagger)\{\lambda_5 H_i H_j H_k S_{ijk}^* + \lambda_9 (H^\dagger H)\mathrm{Tr}(\phi\phi) + \lambda_{10a} S_{ijk}^* S_{ijk}\mathrm{Tr}(\phi\epsilon\phi^T\epsilon^T) \\ & \times \lambda_{10b} S_{ijk}^* S_{ilm} (\epsilon\phi\epsilon^T)_{lj} (\epsilon\phi\epsilon^T)_{mk} + \lambda_{11}[\mathrm{Tr}(\phi\phi)]^2 + \lambda_{12}\mathrm{Tr}(\phi\phi)\mathrm{Tr}(\phi^\dagger\phi) + \mathrm{H.c.}\}. \end{aligned} \tag{A2}$$

Whenever it is appropriate, we use a vector and matrix notation [in $SU(2)_L$ space] for the various fields. As usual, ϵ stands for the two-dimensional Levi-Civita tensor.

[1] Y. Fukuda *et al.* (Super-Kamiokande Collaboration), Evidence for Oscillation of Atmospheric Neutrinos, Phys. Rev. Lett. **81**, 1562 (1998).

[2] Q. Ahmad *et al.* (SNO Collaboration), Direct Evidence for Neutrino Flavor Transformation from Neutral Current Interactions in the Sudbury Neutrino Observatory, Phys. Rev. Lett. **89**, 011301 (2002).

[3] P. F. de Salas, D. V. Forero, C. A. Ternes, M. Tortola, and J. W. F. Valle, Status of neutrino oscillations 2018: 3σ hint for normal mass ordering and improved *CP* sensitivity, Phys. Lett. B **782**, 633 (2018).

[4] P. de Salas, D. Forero, S. Gariazzo, P. Martínez-Miravé, O. Mena, C. Ternes, M. Tórtola, and J. Valle, 2020 Global reassessment of the neutrino oscillation picture, arXiv: 2006.11237.

[5] H. Brown *et al.* (Muon g-2 Collaboration), Precise Measurement of the Positive Muon Anomalous Magnetic Moment, Phys. Rev. Lett. **86**, 2227 (2001).

[6] G. Bennett *et al.* (Muon g-2 Collaboration), Final report of the muon E821 anomalous magnetic moment measurement at BNL, Phys. Rev. D **73**, 072003 (2006).

[7] F. Jegerlehner and A. Nyffeler, The muon g-2, Phys. Rep. **477**, 1 (2009).

[8] P. A. Zyla *et al.* (Particle Data Group), Review of particle physics, Prog. Theor. Exp. Phys. (**2020**), 083C01.

[9] A. Keshavarzi, D. Nomura, and T. Teubner, Muon $g-2$ and $\alpha(M_Z^2)$: A new data-based analysis, Phys. Rev. D **97**, 114025 (2018).

[10] M. Davier, A. Hoecker, B. Malaescu, and Z. Zhang, Reevaluation of the hadronic vacuum polarisation contributions to the Standard Model predictions of the muon $g-2$ and $\alpha(m_Z^2)$ using newest hadronic cross-section data, Eur. Phys. J. C **77**, 827 (2017).

[11] M. Davier, A. Hoecker, B. Malaescu, and Z. Zhang, A new evaluation of the hadronic vacuum polarisation contributions to the muon anomalous magnetic moment and to $\alpha(m_Z^2)$, Eur. Phys. J. C **80**, 241 (2020).

[12] T. Aoyama *et al.*, The anomalous magnetic moment of the muon in the Standard Model, arXiv:2006.04822.

[13] H. Terazawa, All the hadronic contributions to the anomalous magnetic moment of the muon and the lamb shift in the hydrogen atom, Prog. Theor. Phys. **39**, 1326 (1968).

[14] G. Venanzoni (Fermilab E989 Collaboration), The new muon g-2 experiment at Fermilab, Nucl. Part. Phys. Proc. **273–275**, 584 (2016).

[15] M. Otani (E34 Collaboration), Status of the muon g-2/EDM Experiment at J-PARC (E34), J. Phys. Soc. Jpn. Conf. Proc. **8**, 025008 (2015).

[16] S. Borsanyi *et al.*, Leading-order hadronic vacuum polarization contribution to the muon magnetic momentfrom lattice QCD, arXiv:2002.12347.

[17] A. Crivellin, M. Hoferichter, C. A. Manzari, and M. Montull, Hadronic Vacuum Polarization: $(g-2)_\mu$ Versus Global Electroweak Fits, Phys. Rev. Lett. **125**, 091801 (2020).

[18] R. H. Parker, C. Yu, W. Zhong, B. Estey, and H. Müller, Measurement of the fine-structure constant as a test of the Standard Model, Science **360**, 191 (2018).

[19] T. Aoyama, T. Kinoshita, and M. Nio, Revised and improved value of the QED tenth-order electron anomalous magnetic moment, Phys. Rev. D **97**, 036001 (2018).

[20] A. Cárcamo Hernández, S. King, H. Lee, and S. Rowley, Is it possible to explain the muon and electron $g-2$ in a Z' model? Phys. Rev. D **101**, 115016 (2020).

[21] G. Giudice, P. Paradisi, and M. Passera, Testing new physics with the electron $g-2$, J. High Energy Phys. 11 (2012) 113.

[22] A. Crivellin, M. Hoferichter, and P. Schmidt-Wellenburg, Combined explanations of $(g-2)_{\mu,e}$ and implications for a large muon EDM, Phys. Rev. D **98**, 113002 (2018).

[23] I. Doršner, S. Fajfer, and S. Saad, $\mu \to e\gamma$ selecting scalar leptoquark solutions for the $(g-2)_{e,\mu}$ puzzles, arXiv: 2006.11624.

[24] J. Liu, C. E. Wagner, and X.-P. Wang, A light complex scalar for the electron and muon anomalous magnetic moments, J. High Energy Phys. 03 (2019) 008.

[25] B. Dutta and Y. Mimura, Electron $g-2$ with flavor violation in MSSM, Phys. Lett. B **790**, 563 (2019).

[26] M. Bauer, M. Neubert, S. Renner, M. Schnubel, and A. Thamm, Axion-Like Particles, Lepton-Flavor Violation and a New Explanation of a_μ and a_e, Phys. Rev. Lett. **124**, 211803 (2020).
[27] G. Hiller, C. Hormigos-Feliu, D. F. Litim, and T. Steudtner, Anomalous magnetic moments from asymptotic safety, arXiv:1910.14062.
[28] A. Cárcamo Hernández, Y. Hidalgo Velásquez, S. Kovalenko, H. Long, N. A. Pérez-Julve, and V. Vien, Fermion spectrum and $g-2$ anomalies in a low scale 3-3-1 model, arXiv:2002.07347.
[29] C. Hati, J. Kriewald, J. Orloff, and A. Teixeira, Anomalies in ^{8}Be nuclear transitions and $(g-2)_{e,\mu}$: Towards a minimal combined explanation, J. High Energy Phys. 07 (2020) 235.
[30] C.-H. Chen and T. Nomura, Electron and muon $g-2$, radiative neutrino mass, and $\ell' \to \ell\gamma$ in a $U(1)_{e-\mu}$ model, arXiv:2003.07638.
[31] L. Calibbi, M. López-Ibáñez, A. Melis, and O. Vives, Muon and electron $g-2$ and lepton masses in flavor models, J. High Energy Phys. 06 (2020) 087.
[32] F. J. Botella, F. Cornet-Gomez, and M. Nebot, Electron and muon $g-2$ anomalies in general flavour conserving two Higgs doublets models, Phys. Rev. D **102**, 035023 (2020).
[33] K.-F. Chen, C.-W. Chiang, and K. Yagyu, An explanation for the muon and electron $g-2$ anomalies and dark matter, arXiv:2006.07929.
[34] B. Dutta, S. Ghosh, and T. Li, Explaining $(g-2)_{\mu,e}$, KOTO anomaly and MiniBooNE excess in an extended Higgs model with sterile neutrinos, arXiv:2006.01319.
[35] S. Jana, V. P. K., and S. Saad, Resolving electron and muon $g-2$ within the 2HDM, Phys. Rev. D **101**, 115037 (2020).
[36] M. Badziak and K. Sakurai, Explanation of electron and muon $g-2$ anomalies in the MSSM, J. High Energy Phys. 10 (2019) 024.
[37] M. Endo, S. Iguro, and T. Kitahara, Probing $e\mu$ flavor-violating ALP at Belle II, J. High Energy Phys. 06 (2020) 040.
[38] M. Abdullah, B. Dutta, S. Ghosh, and T. Li, $(g-2)_{\mu,e}$ and the ANITA anomalous events in a three-loop neutrino mass model, Phys. Rev. D **100**, 115006 (2019).
[39] K. S. Babu, S. Nandi, and Z. Tavartkiladze, New mechanism for neutrino mass generation and triply charged Higgs bosons at the LHC, Phys. Rev. D **80**, 071702 (2009).
[40] F. Staub, SARAH 3.2: Dirac gauginos, UFO output, and more, Comput. Phys. Commun. **184**, 1792 (2013).
[41] F. Staub, SARAH 4: A tool for (not only SUSY) model builders, Comput. Phys. Commun. **185**, 1773 (2014).
[42] W. Porod, SPheno, a program for calculating supersymmetric spectra, SUSY particle decays and SUSY particle production at e+ e- colliders, Comput. Phys. Commun. **153**, 275 (2003).
[43] W. Porod and F. Staub, SPheno 3.1: Extensions including flavour, *CP*-phases and models beyond the MSSM, Comput. Phys. Commun. **183**, 2458 (2012).
[44] I. Cordero-Carrión, M. Hirsch, and A. Vicente, Master Majorana neutrino mass parametrization, Phys. Rev. D **99**, 075019 (2019).
[45] I. Cordero-Carrión, M. Hirsch, and A. Vicente, General parametrization of Majorana neutrino mass models, Phys. Rev. D **101**, 075032 (2020).
[46] J. Alwall, P. Demin, S. de Visscher, R. Frederix, M. Herquet, F. Maltoni, T. Plehn, D. L. Rainwater, and T. Stelzer, MADGRAPH/MADEVENT v4: The new web generation, J. High Energy Phys. 09 (2007) 028.
[47] J. Alwall, M. Herquet, F. Maltoni, O. Mattelaer, and T. Stelzer, MADGRAPH5: Going beyond, J. High Energy Phys. 06 (2011) 128.
[48] J. Alwall, R. Frederix, S. Frixione, V. Hirschi, F. Maltoni, O. Mattelaer, H. S. Shao, T. Stelzer, P. Torrielli, and M. Zaro, The automated computation of tree-level and next-to-leading order differential cross sections, and their matching to parton shower simulations, J. High Energy Phys. 07 (2014) 079.
[49] A. Manohar, P. Nason, G. P. Salam, and G. Zanderighi, How Bright is the Proton? A Precise Determination of the Photon Parton Distribution Function, Phys. Rev. Lett. **117**, 242002 (2016).
[50] A. V. Manohar, P. Nason, G. P. Salam, and G. Zanderighi, The photon content of the proton, J. High Energy Phys. 12 (2017) 046.
[51] J. Butterworth *et al.*, PDF4LHC recommendations for LHC Run II, J. Phys. G **43**, 023001 (2016).
[52] A. M. Sirunyan *et al.* (CMS Collaboration), Search for physics beyond the standard model in multilepton final states in proton-proton collisions at $\sqrt{s} = 13$ TeV, J. High Energy Phys. 03 (2020) 051.
[53] A. M. Sirunyan *et al.* (CMS Collaboration), Search for Evidence of the Type-III Seesaw Mechanism in Multilepton Final States in Proton-Proton Collisions at $\sqrt{s} = 13$ TeV, Phys. Rev. Lett. **119**, 221802 (2017).